

Nonvolatile ferroelectric control of electronic properties of Bi_2Te_3

Xusheng Ding(丁旭升), Yunfei Li(李云飞), Chaoyang Kang(康朝阳), Ye-Heng Song(宋业恒), and Weifeng Zhang(张伟风)

Citation: Chin. Phys. B, 2024, 33 (**11**): 117301. DOI: 10.1088/1674-1056/ad7670
Journal homepage: http://cpb.iphy.ac.cn; http://iopscience.iop.org/cpb

What follows is a list of articles you may be interested in

Topological superconductors with spin-triplet pairings and Majorana Fermi arcs

Shi Huang(黄石) and Xi Luo(罗熙)
Chin. Phys. B, 2024, 33 (**8**): 087301. DOI: 10.1088/1674-1056/ad462f

Low-damage photolithography for magnetically doped $(Bi,Sb)_2Te_3$ quantum anomalous Hall thin films

Zhiting Gao(高志廷), Minghua Guo(郭明华), Zichen Lian(连梓臣), Yaoxin Li(李耀鑫), Yunhe Bai(白云鹤), Xiao Feng(冯硝), Ke He(何珂), Yayu Wang(王亚愚), Chang Liu(刘畅), and Jinsong Zhang(张金松)
Chin. Phys. B, 2023, 32 (**11**): 117303. DOI: 10.1088/1674-1056/ad0147

Negative magnetoresistance in Dirac semimetal Cd_3As_2 with in-plane magnetic field perpendicular to current

Hao-Nan Cui(崔浩楠), Guang-Yu Zhu(祝光宇), Jian-Kun Wang(王建坤), Jia-Jie Yang(杨佳洁), Wen-Zhuang Zheng(郑文壮), Ben-Chuan Lin(林本川), Zhi-Min Liao(廖志敏), Shuo Wang(王硕), and Da-Peng Yu(俞大鹏)
Chin. Phys. B, 2023, 32 (**7**): 077305. DOI: 10.1088/1674-1056/accd50

Spin transport properties in ferromagnet/superconductor junctions on topological insulator

Hong Li(李红) and Xin-Jian Yang(杨新建)
Chin. Phys. B, 2022, 31 (**12**): 127301. DOI: 10.1088/1674-1056/ac989e

Effects of post-annealing on crystalline and transport properties of Bi_2Te_3 thin films

Qi-Xun Guo(郭奇勋), Zhong-Xu Ren(任中旭), Yi-Ya Huang(黄意雅), Zhi-Chao Zheng(郑志超), Xue-Min Wang(王学敏), Wei He(何为), Zhen-Dong Zhu(朱振东), and Jiao Teng(滕皎)
Chin. Phys. B, 2021, 30 (**6**): 067307. DOI: 10.1088/1674-1056/abee6c

---

Nonvolatile ferroelectric control of electronic properties of Bi_2Te_3

Xusheng Ding(丁旭升), Yunfei Li(李云飞), Chaoyang Kang(康朝阳),
Ye-Heng Song(宋业恒)[†], and Weifeng Zhang(张伟风)[‡]

Henan Key Laboratory of Quantum Materials and Quantum Energy, Center for Topological Functional Materials, School of Future Technology, Henan University, Kaifeng 475004, *China*

(Received 8 May 2024; revised manuscript received 31 August 2024; accepted manuscript online 3 September 2024)

Nonvolatile electric-field control of the unique physical characteristics of topological insulators (TIs) is essential for the fundamental research and development of practical electronic devices. Electrically tunable transport properties through gating materials have been extensively investigated. However, the relatively weak and volatile tunability limits its practical applications in spintronics. Here, we demonstrate the nonvolatile electric-field control of Bi_2Te_3 transport properties via constructing ferroelectric Rashba architectures, i.e., 2D Bi_2Te_3/α-In_2Se_3 ferroelectric field-effect transistors. By switching the polarization states of α-In_2Se_3, the Fermi level, resistance, Fermi wave vector, carrier mobility, carrier density and magnetoresistance (MR) of the Bi_2Te_3 film can be effectively modulated. Importantly, a shift of the Fermi level towards a band gap with a surface state occurs as switching to a negative polarization state, the contribution of the surface state to the conductivity then increases, thereby increasing the carrier mobility and electron coherence length significantly, resulting in the enhanced weak anti-localization (WAL) effect. These results provide a nonvolatile electric-field control method to tune the electronic properties of TI and can further extend to quantum transport properties.

Keywords: topological insulator, weak anti-localization effect, α-In_2Se_3, electrical transport characteristics

PACS: 73.50.–h, 77.84.–s, 81.15.Hi, 72.15.Rn **DOI:** 10.1088/1674-1056/ad7670

1. Introduction

Three-dimensional (3D) topological insulators (TIs) embody a novel state of matter, characterized by a bulk that is insulating and a surface that exhibits metallic properties. This singular trait remains robust due to topological protection.[1,2] This material holds immense potential for applications in data storage, spintronic devices, flexible devices and quantum computing.[3–6] At present, in order to realize the control of relevant quantum effects in 3D TIs, such as Bi_2Te_3, Bi_2Se_3 and Sb_2Te_3, for example, the weak anti-localization (WAL) effect in Sn-doped Bi_2Te_3,[7] researchers have conducted in-depth studies on the element doping,[8] epitaxial strain,[9] dielectric gating[10] and so on. Although the voltage-based manipulation of TI physical characteristics has been successfully demonstrated using dielectric materials, such as Al_2O_3,[11] SiO_2,[12] HfO_2[13] and $SrTiO_3$[14] as the gating layer, the carrier surface density achieved by dielectric materials is relatively small and volatile, preventing the realization of non-volatile carrier regulation and control of related characteristics. Therefore, achieving non-volatile regulation of the physical characteristics of topological insulators is crucial for their practical utilization in fields such as data storage, spintronic devices, flexible electronics and quantum computing.

Certain ferroelectric materials can generate strong local electric fields that change the carrier density of neighboring materials, resulting in greater tunability.[15–17] Among these, α-In_2Se_3 stands out as a non-volatile material where in-plane and out-of-plane ferroelectricities are locked into each other.[18] At present, α-In_2Se_3 is used as a ferroelectric substrate to make various heterojunctions with other functional materials, and related research has been conducted in the fields of ferroelectric storage, optoelectronic devices and flexible devices.[19–21] Leveraging the polarization charge induced by its electric field, α-In_2Se_3 allows for effective and non-volatile modulation of the electric properties. Therefore, the utilization of α-In_2Se_3 as a gating material presents a viable option for achieving non-volatile manipulation of the pertinent physical properties of TI films.

In this study, a Bi_2Te_3/α-In_2Se_3 ferroelectric effect transistor was constructed by growing Bi_2Te_3 thin film on 2D α-In_2Se_3 ferroelectric single crystal. By switching the direction of ferroelectric polarization, the non-volatile voltage control of the Fermi level, resistance, Fermi wave vector, carrier mobility, carrier density and MR in Bi_2Te_3 thin films is successfully achieved. Specifically, when the original state is changed to negative polarization, the Fermi wave vector and carrier density decrease significantly, while the carrier mobility increases significantly, reflecting a shift of the Fermi level towards the band gap with a surface state, resulting in an enhanced WAL effect. However, upon the polarization switching to positive polarization, these transport characteristics change and are completely opposite to negative polarization, indicating that the Fermi energy level shifts deeper into the bulk band.

[†]Corresponding author. E-mail: yehengsong@henu.edu.cn
[‡]Corresponding author. E-mail: wfzhang@henu.edu.cn

© 2024 Chinese Physical Society and IOP Publishing Ltd

2. Experimental details

Bi_2Te_3 thin film was epitaxially grown on a mechanically exfoliated α-In_2Se_3 thin flake using an MBE system. The Bi:Te beam ratio ranged from 1:10 to 1:6, and the system operated under a vacuum of approximately 1.0×10^{-9} mbar. The thin film growth was conducted at substrate temperatures ranging from 190 °C to 220 °C. The Bi_2Te_3 thin film, tested in this study, had a thickness of 10 nm to 12 nm, while the α-In_2Se_3 thin flake was treated as a bulk material. Electrodes were patterned using ultraviolet photolithography and transferred onto the device as top electrodes, with highly doped Si serving as the bottom electrodes. The purity, crystallinity and crystal structure of the Bi_2Te_3 thin film and α-In_2Se_3 thin flake were characterized using Raman spectroscopy. PFM images, hysteresis loops and butterfly curves were obtained using an MFP-3D Infinity atomic force microscope from Asylum Research. The electrical transport properties of the Bi_2Te_3 thin film before and after polarization were measured using a physical properties measurement system (PPMS). The measurements included resistance, Hall resistance and magnetoresistance. The Hall resistance was determined using a four-probe method. Figures 2(f)–2(h) were calculated from the R_{xy} Hall resistance data presented in Figs. 2(b)–2(e). Successively applying ±3 V direct current voltage for 20 min in the thickness direction of the α-In_2Se_3 thin flakes ensures the complete polarization of α-In_2Se_3 and a 180° polarization direction switching.

3. Results and discussion

Figures 1(a) and 1(b) show the structural schematic and optical microscope images of the microdevices, respectively. The device is composed of highly doped Si substrate, mechanically exfoliated α-In_2Se_3 thin flake, Bi_2Te_3 film grown with MBE and Au electrode. The atomic force microscopy (AFM) image (Fig. 1(c)) shows the morphology of Bi_2Te_3 grown by means of MBE. The device is triangular and a spiral grows along the z axis, which demonstrates the excellent crystal quality of Bi_2Te_3. To confirm its crystal structure, we characterized the sample using Raman spectroscopy to demonstrate the macroscopic uniformity and quality of the sample. In Fig. 1(d), we present the Raman spectra of α-In_2Se_3 and Bi_2Te_3 grown on α-In_2Se_3. Bi_2Te_3 exhibits two characteristic peaks centered at 105 cm^{-1} and 137 cm^{-1}, consistent with the previous report,[22] while α-In_2Se_3 shows four distinctive peaks at 92 cm^{-1}, 106 cm^{-1}, 182 cm^{-1} and 201 cm^{-1}.[23] The slight blueshift observed in the Raman spectrum of mechanically exfoliated α-In_2Se_3, compared to previous relevant reports, confirms that our α-In_2Se_3 belongs to the $R3m$ space group. The excellent ferroelectric properties of In_2Se_3 were also confirmed by piezoresponse force microscopy (PFM) (see Fig. S1).

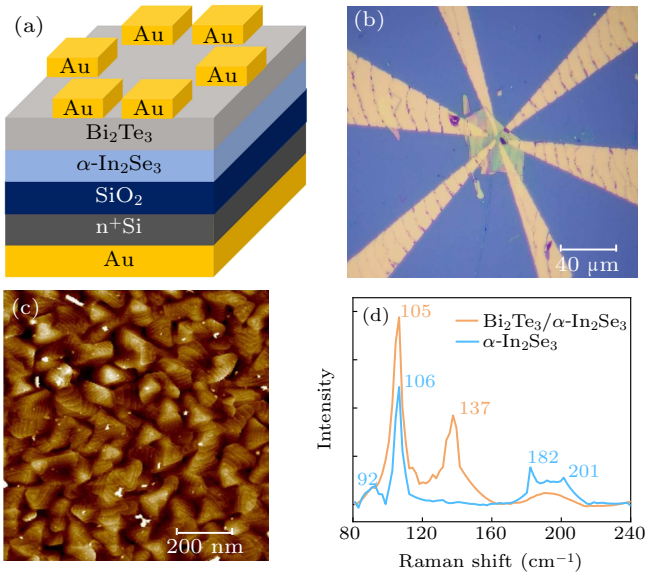


Fig. 1. Microdevice fabrication and characterization. (a) Structural schematic. (b) Optical microscope images. (c) AFM image of a Bi_2Te_3 film. (d) Raman spectra of Bi_2Te_3 film and In_2Se_3 flake, respectively, with 532 nm laser excitation.

To verify the impact of polarization switching on the transport characteristics of the Bi_2Te_3 film, we tested the temperature dependence of the resistance concerning positive and negative polarizations of α-In_2Se_3. Relative to the pre-polarization state, as shown in Fig. 2(a), the resistance of the Bi_2Te_3 film decreases overall after positive polarization. At temperatures $\geq$10 K, the resistance exhibits metallic behavior, with a slight increase in resistance within the 2 K–10 K temperature range. When switching from positive to negative polarization, the resistance decreases overall, but the increase in resistance is more pronounced at temperatures $\leq$ 10 K. Regardless of the polarization before and after, the resistance "increase" that occurs at temperatures below 10 K can be attributed to the electron–electron interaction.[24]

We also performed temperature-dependent Hall measurements on the samples. Some of the measurement results are shown in Figs. 2(b)–2(e). Taking temperature as a variable, the slopes of all R_{xy} are basically unchanged compared to at 2 K and 20 K. The R_{xy} slope of positive polarization decreases from 50 K to 100 K, and the R_{xy} slope of negative polarization increases greatly at 100 K. This is consistent with the trend of change in Figs. 2(f)–2(h). The Hall resistance always exhibits a negative slope in the magnetic field curve, indicating that the Bi_2Te_3 thin film is an n-type semiconductor material with electrons as the majority carriers (the R_{xy} curves of the non-polarized and positively polarized states in Figs. 2(b) and 2(c) almost overlap). Since we measured the transport properties of Bi_2Te_3 film, and considering that the band gaps of Bi_2Te_3 and α-In_2Se_3 are 0.13 eV and 1.3 eV, respectively, this bandgap difference can be regarded as no contribution of α-In_2Se_3 thin films to the transport results. The α-In_2Se_3 in the device can

tune the interface properties of the Bi_2Te_3 film via ferroelectrically polarization. As shown in Figs. 2(f)–2(h), the Fermi wave vector k_F, surface carrier density n_{2D} and carrier mobility μ of the unpolarized Bi_2Te_3 film are basically unchanged throughout the temperature range from 2 K to 100 K. However, after ferroelectric polarization, the above three parameters are significantly changed.

Burrahlek[25] and Chen[10] *et al.* suggest that the increase and decrease of Fermi wave vector k_F reflect the moving direction of the Fermi level, and the movement of the Fermi level will result in the change of the carrier density and carrier mobility, as shown in Figs. 2(g) and 2(h). In Fig. 2(f), k_F in the negative polarization state decreases overall, indicating that the Fermi level of Bi_2Te_3 moves towards the surface state in the bulk band gap, and the surface state crosses it. Then, the surface carrier density and carrier mobility decrease and increase, respectively, compared to the original state. However, for k_F in the positive polarization state (orange-yellow curve in Fig. 2(f)), it remains almost unchanged from 2 K to 20 K, and increases slowly from 20 K to 100 K, which indicates the Fermi level movement to the bulk state. The corresponding carrier density and carrier mobility also change with the same trend of k_F (see Figs. 2(g) and 2(h)).

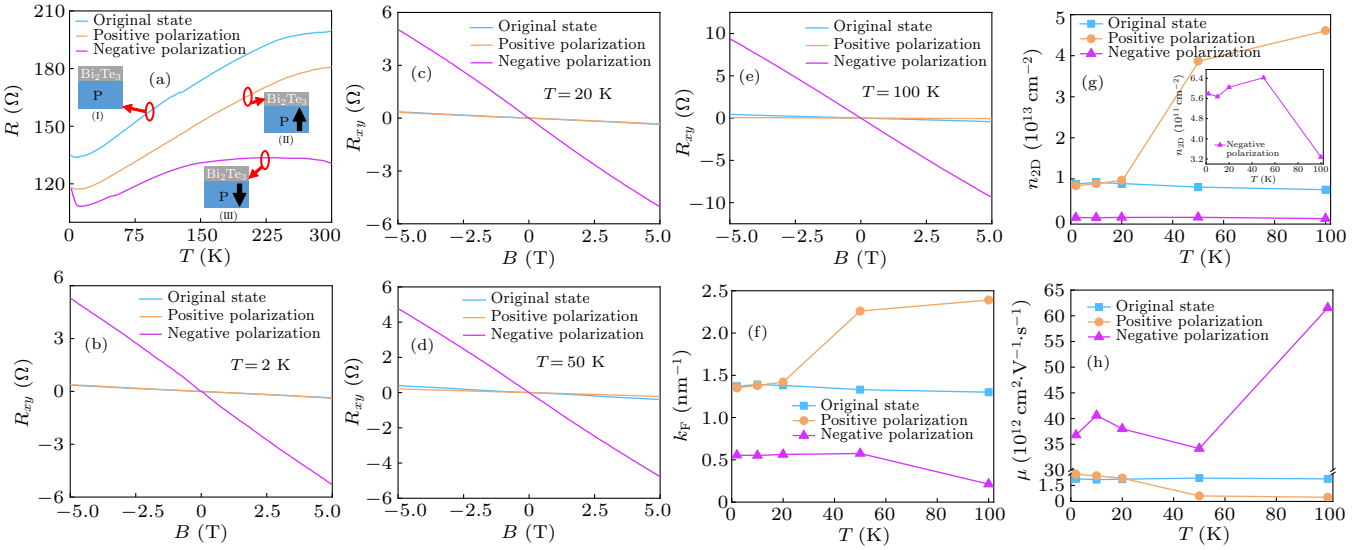


Fig. 2. The resistance and R_{xy} of Bi_2Te_3 film when α-In_2Se_3 is in the original, positive and negative polarization state, respectively, and the data extracted according to R_{xy}. (a) Temperature dependence of the resistance. Insets (I, II, III): Schematic diagrams for the polarization states of the α-In_2Se_3 substrate. (b)–(e) The R_{xy} at 2 K, 10 K, 20 K, 50 K and 100 K, respectively. Fermi wave vector (f), sheet carrier density (g) and carrier mobility (h) of Bi_2Te_3 thin films as a function of temperature with different polarization states of α-In_2Se_3. Inset: Sheet carrier density of the negative polarization states.

The change of the surface carrier density induced by ferroelectric polarization can have a dramatic impact on the MR of the Bi_2Te_3 film. Figures 3(a)–3(d) present the MR at several different temperature points. MR can be defined as $\frac{R(B)-R(0)}{R(0)} \times 100\%$, where $R(B)$ and $R(0)$ correspond to the resistance of the Bi_2Te_3 film under the influence of an applied vertical magnetic field and the absence of a magnetic field, respectively. As shown in Figs. 3(a)–3(c), the MR drops dramatically with the decrease in the magnetic field, showing a sharp WAL peak at temperatures $\leq$ 20 K nearing zero magnetic fields. This is a signature of WAL effects, attributed to destructive quantum interference or the suppression of carrier backscattering.[26] In Fig. S2, as the temperature rises to 50 K and 100 K, the peaks are suppressed and transform into a broad angular shape. Interestingly, when the ferroelectric polarization of α-In_2Se_3 undergoes a transition from positive to negative polarization, it results in an enhancement of the WAL effect, which is manifested by an increase in the MR value of the low magnetic field and narrowing of the WAL peak in Figs. 3(a)–3(d). This phenomenon is particularly evident at 2 K under negative polarization (Fig. 3(a)). As shown in Fig. 3(d), the low-field ($\pm$1 T) MR of negative polarization exhibits a sharper spike compared with the positive polarization and Bi_2Te_3 itself at the same temperature, indicating an enhanced WAL effect and increased electron-phase coherence length. These results demonstrate the high effectiveness of in situ carrier density modulation on magnetic transport characteristics via a nonvolatile manner by controlling the polarization states.

In order to further understand the WAL effect, we used the simplified formula of Hikami–Larkin–Nagaoka (HLN)[27] to convert the magnetoresistance of the low magnetic field ($\pm$1 T) region into the unit permeability for fitting, and the results are shown in Figs. 4(a)–4(d). According to this formula, the permeability correction caused by the WAL effect can be described as

$$\Delta G = \alpha \frac{e^2}{2\pi^2\hbar}\left[\Psi\left(\frac{1}{2}+\frac{\hbar}{4eBL_\varphi^2}\right)-\ln\left(\frac{\hbar}{4eBL_\varphi^2}\right)\right],$$

where the prefactor α is the fitting parameter, Ψ is the dou-

ble gamma function, $\hbar$ is the reduced Planck constant, B is the magnetic field and L_φ is the phase coherence length. When α-In_2Se_3 is in the negative polarization state, the absolute value of the relative change of the magnetic conductivity of Bi_2Te_3 films is greater than that in the positive polarization state between 2 K and 20 K. Figures 4(e) and 4(f) show the α and L_φ parameters in the HLN formula. The α value is about $\sim 1.2 \times 10^5$, which has no specific physical significance. This is due to the large α value caused by the three-dimensional or bulk contribution of the material and multiple conduction channels.[28–31] The results show that when α-In_2Se_3 substrate is in the negative polarization state at low temperature, the inclusion of a carrier will increase the time inversion symmetric channel of Bi_2Te_3 film, and the quantum interference phenomenon will be enhanced. Moreover, with the increase in temperature, the enhancement of electron–phonon and electron–electron inelastic scattering in the film state will destroy the quantum interference phenomenon, and the difference between the phase coherence lengths will decrease at different polarization states, and almost overlap at 50 K.

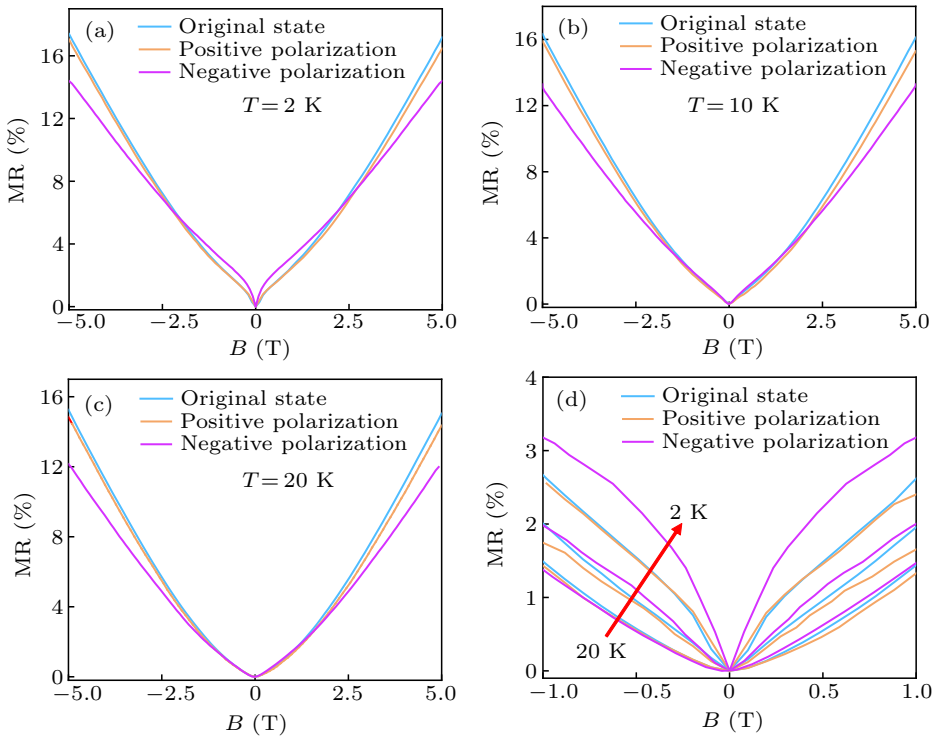


Fig. 3. Normalized MR of Bi_2Te_3 films with α-In_2Se_3 substrate in the original, positive and negative polarization state, respectively. The direction of the magnetic field is perpendicular to the film plane and electric current ($B_\perp$). (a)–(c) MR of the Bi_2Te_3 film as a function of magnetic fields at fixed temperatures. (d) MR at different temperatures with ±1 T magnetic field.

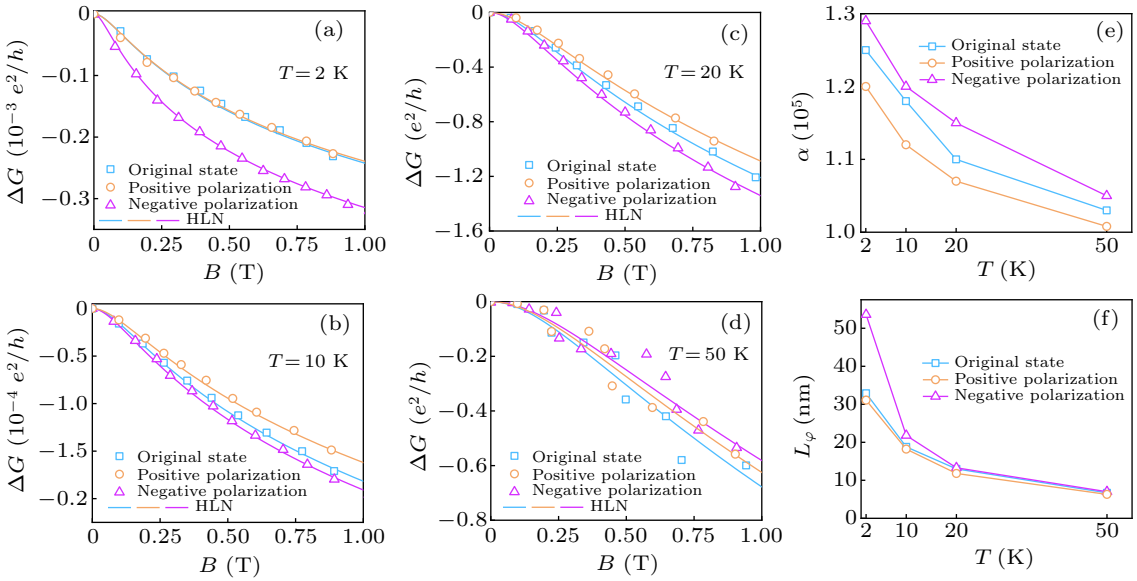


Fig. 4. In the three states of the α-In_2Se_3 substrate, the conductivity of Bi_2Te_3 film changes with the change of magnetic field. The solid line is the result obtained by fitting the HLN formula, and the scatter plot (data points) represents the actual measurement results. (a) 2 K, (b) 10 K, (c) 20 K, (d) 50 K. Then, the relationship between parameters (e) α and (f) L_φ with temperature is fitted.

Based on the above transport measurement results, we propose a band structure evolution diagram (see Fig. 5) with different polarization states to explain the observed experimental results. According to the work of Shekhar,[32] Liang[33] and Shrestha,[34] the shift of Fermi level leads to the change of carrier mobility that can affect the strength of the WAL effect. The WAL effect of topological insulators is mainly contributed by the topological surface states with strong spin–orbit coupling. It is assumed that the Fermi level of this Bi_2Te_3 film is in its bulk band when it is without polarization (see the middle panel in Fig. 5). Compared with the original state, the positively polarized state first causes the Fermi level to shift to the bulk band above 20 K. The position of the Fermi level in the positive polarization state only moves upwards a little compared to the original state, resulting in decreased carrier mobility (Fig. 2(h)) and increased surface carrier density (Fig. 2(g)). In this case, the bulk state electrons contribute more to the conductance, leading to a smaller electron correlation length, thus weakening the WAL effect. In the temperature range of 2 K–20 K, we suggest that the low temperature may limit the thermal motion of electrons and make the Fermi level return to a position similar to that of the original state, thus showing a similar surface carrier density and mobility. For the negative polarization, it causes the Fermi level to shift to the bulk band gap with the surface state in the entire measured temperature range (see Fig. 5). At the same time, there is an enhancement in the contribution of surface states towards conductivity, resulting in deceased carrier density and increased carrier mobility, which agrees well with the experimental results (see Figs. 2(g) and 2(h)). At the same time, the electron coherence length also increases, leading to the enhancement of WAL, which in magnetoresistive measurement is represented by a narrowing of MR spikes around the zero magnetic field (see Fig. 3(a)).

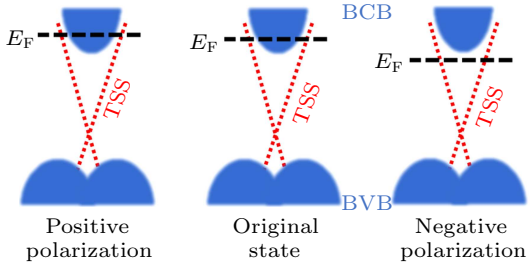


Fig. 5. From left to right, the figure displays the changes in the Fermi energy level in the positively polarized state, the original (or unpolarized) state and the negatively polarized state.

4. Conclusion

In summary, we fabricated a Bi_2Te_3/α-In_2Se_3 ferroelectric field-effect device. The effect of ferroelectric polarization switching on the electronic properties of Bi_2Te_3 thin films was studied. The results indicate that the Fermi level, resistance, Fermi wave vector, carrier mobility, carrier density and MR can be in situ modulated in a non-volatile way by switching between different polarization states of α-In_2Se_3. When switching to positive polarization, there is a shift of the Fermi level towards the bulk bands, inducing increased Fermi wave vector and carrier density, and decreased carrier mobility. However, when switching from positive to negative polarization, these transport properties undergo opposite changes to those observed with positive polarization. Both the Fermi wave vector and carrier density decrease significantly, while the carrier mobility increases significantly, reflecting a shift of the Fermi level towards the band gap with a surface state. The influence of surface states on conductivity has intensified, making the phase coherence length larger, so that an enhanced WAL effect is observed. Our findings suggest that the use of α-In_2Se_3 as substrates and gating materials for voltage-controlled transport properties of TIs can be extended to the study of carrier-related quantum transport properties in other quantum materials, such as topological superconductors and Dirac semimetals. This method allows better understanding of the quantum transport properties related to carrier transport in three-dimensional TI films.

Data availability statement

The data that support the findings of this study are available from the corresponding author upon reasonable request.

Acknowledgements

Project supported by the National Natural Science Foundation of China (Grant Nos. 12004099 and 11974099), the Zhongyuan Leading Talents, Plan for Leading Talent of Fundamental Research of the Central China in 2020, and the Intelligence Introduction Plan of Henan Province in 2021 (Grant No. CXJD2021008).

References

[1] Moore J E 2010 *Nature* **464** 7286
[2] Qi X L and Zhang S C 2010 *Phys. Today* **63** 33
[3] Ngabonziza P, Stehno M P, Myoren H, Neumann V A, Koster G and Brinkman A 2016 *Adv. Electron. Mater.* **2** 1600157
[4] He L, Xiu F, Wang Y, Fedorov A V, Huang G, Kou X, Lang M, Beyermann W P, Zou J and Wang K L 2011 *J. Appl. Phys.* **109** 103702
[5] Mellnik A R, Lee J S, Richardella A, Grab J L, Mintun P J, Fischer M H, Vaezi A, Manchon A, Kim E A, Samarth N and Ralph D C 2014 *Nature* **511** 7510
[6] Li C H, van 't Erve O M, Li Y Y, Li L and Jonker B T 2016 *Sci. Rep.* **6** 29533
[7] Zhang H B, Yu H L, Bao D H, Li S W, Wang C X and Yang G W 2012 *Phys. Rev. B* **86** 075102
[8] Chen Y L, Chu J H, Analytis J G, Liu Z K, Igarashi K, Kuo H H, Qi X L, Mo S K, Moore R G, Lu D H, Hashimoto M, Sasagawa T, Zhang S C, Fisher I R, Hussain Z and Shen Z X 2010 *Science* **329** 659
[9] Liu Y, Li Y Y, Rajput S, Gilks D, Lari L, Galindo P L, Weinert M, Lazarov V K and Li L 2014 *Nat. Phys.* **10** 294

[10] Chen J, Qin H J, Yang F, Liu J, Guan T, Qu F M, Zhang G H, Shi J R, Xie X C, Yang C L, Wu K H, Li Y Q and Lu L 2010 *Phys. Rev. Lett.* **105** 176602

[11] Liu H and Ye P D 2011 *Appl. Phys. Lett.* **99** 084104

[12] Kong D, Dang W, Cha J J, Li H, Meister S, Peng H, Liu Z and Cui Y 2010 *Nano Lett.* **10** 2245

[13] Steinberg H, Laloë J B, Fatemi V, Moodera J S and Jarillo-Herrero P P 2011 *Phys. Rev. B* **84** 23

[14] Zhang G, Qin H, Chen J, He X, Lu L, Li Y and Wu K 2011 *Adv. Funct. Mater.* **21** 2351

[15] Yan J M, Xu Z X, Chen T W, Xu M, Zhang C, Zhao X W, Liu F, Guo L, Yan S Y, Gao G Y, Wang F F, Zhang J X, Dong S N, Li X G, Luo H S, Zhao W and Zheng R K 2019 *ACS Appl. Mater. Inter.* **11** 9548

[16] Zhu Q X, Yang M M, Zheng M, Zheng R K, Guo L J, Wang Y, Zhang J X, Li X M, Luo H S and Li X G 2015 *Adv. Funct. Mater.* **25** 1111

[17] Yan M Y, Yan J M, Zhang M Y, Chen T W, Gao G Y, Wang F F, Chai Y and Zheng R K 2020 *Appl. Phys. Lett.* **117** 23

[18] Xue F, Hu W, Lee K C, Lu L S, Zhang J, Tang H L, Han A, Hsu W T, Tu S, Chang W H, Lien C H, He J H, Zhang Z, Li L J and Zhang X 2018 *Adv. Funct. Mater.* **28** 1803738

[19] Si M, Saha A K, Gao S, Qiu G, Qin J, Duan Y, Jian J, Niu C, Wang H, Wu W, Gupta S K and Ye P D 2019 *Nat. Electron.* **2** 580

[20] Li Y, Chen C, Li W, Mao X, Liu H, Xiang J, Nie A, Liu Z, Zhu W and Zeng H 2020 *Adv. Electron. Mater* **6** 2000061

[21] Si M, Zhang Z, Chang S C, Haratipour N, Zheng D, Li J, Avci U E and Ye P D 2021 *ACS Nano* **15** 5689

[22] Wang K, Liu Y, Wang W, Meyer N, Bao L H and He L 2013 *Appl. Phys. Lett.* **103** 031605

[23] Wan S, Li Y, Li W, Mao X, Zhu W and Zeng H 2018 *Nanoscale* **10** 14885

[24] Lu H Z and Shen S Q 2014 *Phys. Rev. Lett.* **112** 146601

[25] Brahlek M, Koirala N, Bansal N and Oh S 2015 *Solid State Commun.* **215** 54

[26] Yan M Y, Li S S, Yan J M, Xie L, Xu M, Guo L and Zhang S J 2022 *Phys. Rev. Appl.* **18** 044073

[27] Hikami S, Larkin A I and Nagaoka Y 1980 *Progress of Theoretical Physics* **63** 707

[28] Malick S, Sarkar A B, Laha A, Anas M, Malik V K, Agarwal A, Hossain Z and Nayak J 2022 *Phys. Rev. B* **106** 075105

[29] Laha A, Malick S, Singha R, Mandal P and Hossain Z 2019 *Phys. Rev. B* **99** 241102

[30] Zhang J, Hou Z, Zhang C, Chen J and Zhang X 2019 *Appl. Phys. Lett.* **115** 172407

[31] Malick S, Ghosh A, Barman C K, Alam A and Nayak J 2022 *Phys. Rev. B* **105** 165105

[32] Chen Z, Yuan H, Zhang Y, Nomura K, Gao T, Gao Y, Shimotani H, Liu Z and Iwasa Y 2012 *Nano Lett.* **12** 2212

[33] Liang T, Gibson Q, Ali M N, Liu M, Cava R J and Ong N P 2014 *Nat. Mater.* **14** 280

[34] Shrestha K, Chou M, Graf D, Yang H D, Lorenz B and Chu C W 2017 *Phys. Rev. B* **95** 195113